

Tunable terahertz chiral response in all-dielectric BIC metasurfaces

YANG Yue, YAO Bu-yi, DAI Hai-tao, HAO Xi-chen, WANG Yu-han, WANG Ruo-tong, GUO Ting-yang, DU Wen, GAO Ming, TAN Qi, LI Ji-ning, YAO Jian-quan

Citation:

YANG Yue, YAO Bu-yi, DAI Hai-tao, HAO Xi-chen, WANG Yu-han, WANG Ruo-tong, GUO Ting-yang, DU Wen, GAO Ming, TAN Qi, LI Ji-ning, YAO Jian-quan. Tunable terahertz chiral response in all-dielectric BIC metasurfaces[J]. *Chinese Optics*, In press. doi: 10.37188/CO.EN-2025-0045

杨悦, 姚不已, 戴海涛, 郝希晨, 王雨涵, 王若同, 郭廷扬, 杜文, 高铭, 谭琪, 李吉宁, 姚建铨. 基于BIC的全介质太赫兹手性可调超表面[J]. *中国光学*, 优先发表. doi: 10.37188/CO.EN-2025-0045

View online: <https://doi.org/10.37188/CO.EN-2025-0045>

Articles you may be interested in

[Independent dual-band bound states in the continuum based on terahertz all-dielectric metasurfaces](#)

基于太赫兹全介质超表面的独立双带连续域束缚态

Chinese Optics. 2025, 18(5): 1230 <https://doi.org/10.37188/CO.EN-2025-0004>

[Terahertz broadband absorption spectrum enhancement based on asymmetric dielectric meta-grating on a metal substrate](#)

基于金属基底非对称介质超光栅的太赫兹宽带吸收谱增强

Chinese Optics. 2025, 18(4): 738 <https://doi.org/10.37188/CO.2024-0197>

[Bandwidth-tunable terahertz metamaterial half-wave plate component](#)

带宽可调谐的太赫兹超构材料半波片器件

Chinese Optics. 2023, 16(3): 701 <https://doi.org/10.37188/CO.2022-0198>

[Tunable reflective spin-decoupled encoding metasurface based on Dirac semimetals](#)

基于狄拉克半金属的可调谐反射自旋解耦编码超表面

Chinese Optics. 2025, 18(4): 968 <https://doi.org/10.37188/CO.EN-2024-0037>

[Terahertz band-stop filter with H-type structure](#)

类H型结构的太赫兹带阻滤波器

Chinese Optics. 2024, 17(4): 757 <https://doi.org/10.37188/CO.2023-0179>

[Recent advances in metasurfaces for polarization imaging](#)

面向偏振成像的超构表面研究进展

Chinese Optics. 2023, 16(5): 973 <https://doi.org/10.37188/CO.2022-0234>

文章编号 2097-1842(xxxx)x-0001-09

Tunable terahertz chiral response in all-dielectric BIC metasurfaces

YANG Yue¹, YAO Bu-yi^{2*}, DAI Hai-tao^{2*}, HAO Xi-chen², WANG Yu-han², WANG Ruo-tong²,
GUO Ting-yang², DU Wen², GAO Ming², TAN Qi³, LI Ji-ning³, YAO Jian-quan^{3*}

(1. School of Computer and Information Engineering, Tianjin Chengjian University, Tianjin 300384, China;

2. Tianjin Key Laboratory of Low Dimensional Materials Physics and Preparing Technology,
School of Science, Tianjin University, Tianjin 300072, China;

3. School of Precision Instruments and Opto-Electronics Engineering, Tianjin University,
Tianjin, 300072, China)

* Corresponding author, E-mail: yaobuyi@tju.edu.cn; htdai@tju.edu.cn; jqyao@tju.edu.cn

Abstract: Chiral metasurfaces play critical role in physics, materials science, pharmacognosy, and communications. To achieve high-performance chiral responses, such as high circular dichroism (CD) and high-quality factors (Q-factors), BIC-based metasurfaces have been extensively studied as a promising platform. However, most realized BIC metasurfaces rely on metallic constituents whose high electromagnetic losses and absence of dynamic chirality tuning together impose a severe limit on their practical potential. This paper presents an all-dielectric chiral BIC metasurface. By illumination symmetry breaking, the metasurface exhibits a CD value of 0.93. Additionally, dynamic tuning of CD is enabled by external optical pumping. This scheme provides a new avenue for dynamically manipulating the chiral metasurface, which can be used to achieve more complex dynamic chiral characterization and applications.

Key words: all-dielectric metasurface; circular dichroism; dynamic control; terahertz

基于 BIC 的全介质太赫兹手性可调超表面

杨悦¹, 姚不已^{2*}, 戴海涛^{2*}, 郝希晨², 王雨涵², 王若同², 郭廷扬², 杜文², 高铭²,
谭琪³, 李吉宁³, 姚建铨^{3*}

(1. 天津城建大学计算机与信息工程学院, 天津 300384, 中国;

2. 天津大学理学院, 天津市低维材料物理与制备技术重点实验室, 天津 300072, 中国;

3. 天津大学精密仪器与光电工程学院, 天津 300072, 中国)

摘要: 手性超表面在物理学、材料科学、药用植物学和通信领域发挥着关键作用。为实现高性能手性响应(如高圆二色性(CD)和高品质因数(Q因子)), 基于 BIC 的超表面作为极具前景的平台已被广泛研究。然而, 现有的 BIC 超表面大多依赖金属结构, 其高电磁损耗与动态手性调节能力的缺失共同限制了实际应用价值。本文提出一种全介质手性 BIC 超表

收稿日期: 2025-11-27; 修订日期: xxxx-xx-xx

基金项目: 国家自然科学基金(No. 62201378, No. 62375200, No. 12274319)资助

Supported by the National Natural Science Foundation of China (No. 62201378, No.62375200, No.12274319)

面。通过光照对称性破缺,该超表面展现出 0.93 的圆二色性值。此外,通过调节外部泵浦光能够实现圆二色性的动态调谐。该方案为动态操控手性超表面开辟了新途径,可用于实现更复杂的动态手性特性表征与应用。

关键词: 全介质超表面;圆二色性;动态控制;太赫兹

中图分类号: 文献标志码:A **doi:** 10.37188/CO.EN-2025-0045 **CSTR:** 32171.14.CO.EN-2025-0045

1 Introduction

Chirality is a common symmetry in nature that plays a key role in physics, materials science, pharmacognosy, and communication^[1-2]. However, chiral analysis through conventional optical devices is often difficult, because the chiral signal of natural materials is usually weak^[3]. Over the past decades, metasurfaces, a novel type of optical device, have been established as an important research issue for light field manipulation^[4]. By introducing asymmetric units and tailoring the geometric size of the unit cells, metasurfaces can exhibit significant chiral response, which is regarded as a new research direction to enhance chirality^[5]. Current chiral metasurfaces are predominantly based on two approaches: (i) intrinsic chiral meta-atoms through electromagnetic dipole coupling^[6-7], and (ii) achiral meta-atom arrays with phase matrix design^[8]. However, both strategies suffer from limited chirality ($CD < 0.4$) that restricts practical implementations^[9]. Consequently, designing metasurfaces with significantly enhanced chirality using novel mechanisms has become a major focus within the field^[10-11].

BIC, a special type of quantum state in physics, refers to the existence of localized states in a system whose energy is in the continuous spectral range^[12-13]. BIC metasurfaces are optical metasurface systems designed based on the BIC mechanism^[14-15], with a core configuration of periodic nanostructures with specific symmetry breaking^[16]. Since its experimental validation in 2017, it has become a cutting-edge topic in the field of chiral metasurfaces due to its extremely high Q-factor, chiral response, high sensitivity, and other characteristics^[17]. In 2020, Liang et al. proposed a type of anisotropic plasmonic metasurfaces supporting

high-Q resonances associated with quasi-BIC collective lattice modes^[18]. In 2022, Liu et al. proposed an aluminum-based metasurface utilizing symmetry-protected BICs, demonstrating exceptional sensitivity in the THz band^[19]. Despite notable advancements in recent years, most of the metasurfaces used to excite these quasi-BICs with high chirality are asymmetric metal structures, such as pairs of tilted nanobars^[20-21], asymmetric nanorods^[22-23], and split resonant rings^[24-26], which have significant electromagnetic dissipation and suffer from extra scattering losses from the near-field coupled structures^[23]. These intrinsic limitations substantially hinder the practical applicability of such metasurfaces across diverse photonic systems.

In this study, a strength-tunable all-dielectric metasurface with giant chirality in the THz band is proposed. The metasurface employs quartz as the substrate and patterned high-resistivity silicon as the periodic resonant meta-atoms. The symmetric meta-atoms exhibit no extrinsic chirality under normal conditions. Quasi-BICs are induced by oblique incidence, breaking illumination symmetry and resulting in giant CD at the target frequency. Simultaneously, by modulating the conductivity of silicon using a pump beam, the CD value can be dynamically tuned from its maximum to zero. This scheme provides a new avenue for dynamically manipulating the chiral metasurface, which can be used to achieve more complex dynamic chiral characterization and applications.

2 Simulation

2.1 Materials

The substrate is made of quartz (SiO_2), and the square pillars are made of high-resistivity photo-sensitive silicon (HRPS-Si). All materials are from

the CST Studio standard material library.

2.2 Simulation configuration

All transmittance simulations of the metasurface were performed with CST Studio Suite 2019, employing a plane-wave excitation and a field probe positioned at the center above the structure; the bound-state-in-continuum (BIC) analyses were carried out in COMSOL Multiphysics using the Electromagnetic Waves interface.

3 Results and Discussion

As illustrated in Fig. 1(a), the all-dielectric metasurface is composed of periodically arranged square-slotted structures. The substrate is fabricated from quartz (SiO_2), while the slotted square pillars are constructed with high-resistivity photosensitive silicon (HRPS-Si). Fig. 1(b) and Fig. 1(c) present the detailed meta-unit configuration with precise dimensional parameters: the quartz substrate exhibits a thickness H_2 of $100 \mu\text{m}$, the structural period (P) is $150 \mu\text{m}$, and each silicon pillar demonstrates a height H_1 of $100 \mu\text{m}$ with lateral dimensions $L_1 = 120 \mu\text{m}$. The symmetrical slot positioned along the central axis of the silicon pillar measures $L_2 = 60 \mu\text{m}$ in length and $L_3 = 10 \mu\text{m}$ in width.

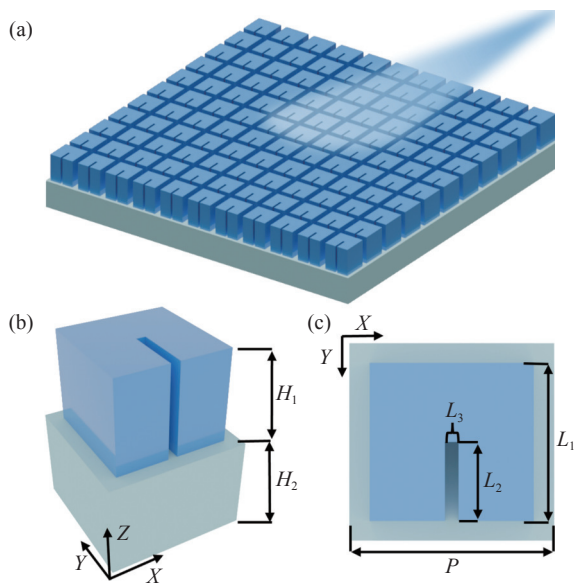


Fig. 1 (a) Schematic diagram of the all-dielectric metasurface. (b) The three-dimensional view and (c) top view of the unit structure.

This material combination leverages the inherent advantages of HRPS-Si, including its elevated resistivity and tunable dielectric properties, coupled with quartz's low-loss characteristics at THz frequency, exceptional thermal stability, and high mechanical strength. These properties collectively enhance the metasurface's operational performance in high-frequency regimes. Moreover, the proposed structure simplifies design workflows through symmetry optimization and minimizes manufacturing tolerances through structural optimization.

To investigate potential BIC eigenstates within the structure, wide-range frequency-spectrum scans are performed with the commercial finite-element solver COMSOL Multiphysics, seeking eigenstates that remain decoupled from all radiation channels in the continuum. As shown in Fig. 2(a) and (b), the dispersion curves and electric field excitations at the three characteristic frequencies reveal signatures indicative of BIC. The dispersion curve of Mode 1 lies between Modes 2 and 3. Moreover, the electric field distributions indicate that Modes 2 and 3 do not exhibit strong localization, representing normal radiative states. In contrast, Mode 1 demonstrates intense electric field localization. Therefore, there are strong reasons to suspect that Mode 1 represents a BIC. The most definitive evidence for BIC is the theoretically predicted infinite Q-factor at the center of the Brillouin zone (Γ point). Therefore, the Q-factor of all three modes was systematically characterized. As shown in Fig. 2(c), Mode 1 displays a pronounced Q-factor peak at the Γ point, providing conclusive verification of BIC existence. Furthermore, to validate the occurrence of the BIC, the polarization topology map of the eigenmode was calculated. As shown in Fig. 2(d), a vector polarization singularity (V-point, indicated by a black dot) is observed at the Γ point, confirming the existence of the symmetry-protected BIC. When in-plane symmetry is broken by introducing oblique illumination, the V-point representing the BIC splits into a pair of circular polarization singularities (C-points, marked by red and

blue dots) with opposite handedness, giving rise to CD response.

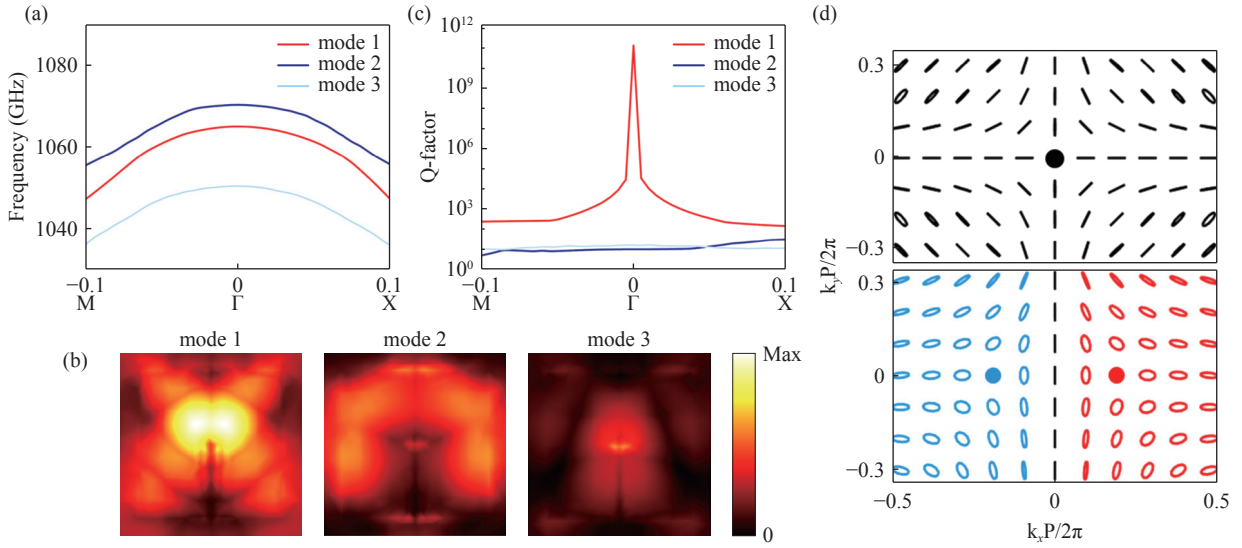


Fig. 2 (a) Dispersion curves of the three modes in k-space. (b) The distribution of excited electric fields within the metasurface unit. (c) Q-factor profiles of the three modes. (d) Eigenpolarization maps.

Following confirmation of the BIC existence, oblique-incidence-induced illumination symmetry breaking was employed to generate quasi-BICs (q-BICs) and concomitant chirality. As shown in Fig. 3(a), under normal incidence (incident angle $\theta=0^\circ$), the metasurface exhibits two resonance peaks in y-polarized spectra aligned with the slot

orientations, whereas no resonance peaks are observed in the x-polarized direction. Moreover, in the circularly polarized transmission spectra shown in Fig. 3(b), both T_{ll} and T_{rr} demonstrate equal magnitudes, as do T_{rl} and T_{lr} , indicating that the metasurface lacks chirality under normal incidence conditions.

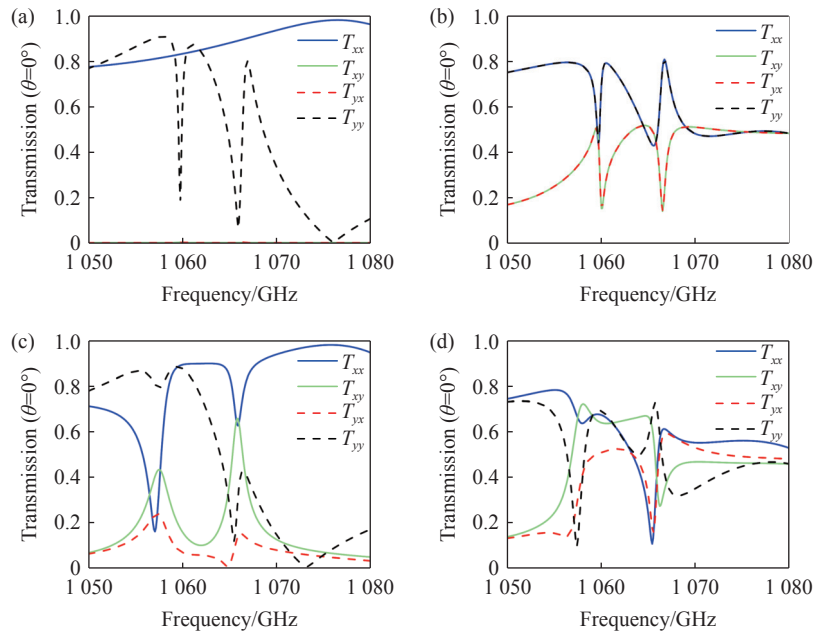


Fig. 3 (a) The linearly polarized transmission spectra and (b) circularly polarized transmission spectra of the metasurface (incident angle $\theta=0^\circ$). (c) The linearly polarized transmission spectra and (d) circularly polarized transmission spectra of the metasurface (incident angle $\theta=4^\circ$).

Corresponding to the case of oblique incidence $\theta = 4^\circ$, in Fig. 3(c), the linearly polarized transmission spectra exhibit a significant difference from those under normal incidence, displaying significant cross-polarization phenomena. In Fig. 3(d), the circularly polarized transmission spectra reveal pronounced minima for T_{rr} and T_{lr} near the target frequency point, while the opposing components T_{ll} and T_{rl} show maxima. This configuration leads to a remarkable chiral transmission phenomenon.

To further elucidate this chiral transmission phenomenon, electric- and magnetic-field excitations at the target frequency are characterized under both incident conditions, as illustrated in Fig. 4(a)

and (b). Under normal incidence (incident angle $\theta = 0^\circ$), both field excitations exhibited significant chiral insensitivity. In contrast, under oblique incidence conditions (incident angle $\theta = 4^\circ$), both the electric and magnetic fields demonstrated predominant right circular polarization (RCP) excitation, which corresponds to the strong resonant peak of the RCP transmission coefficient at the target frequency point in Fig. 4(c). Fig. 4(d) further presents the CD values under both incidence angles. The metasurface maintains $CD = 0$ under normal incidence while achieving a maximum $CD = 0.93$ under oblique incidence conditions.

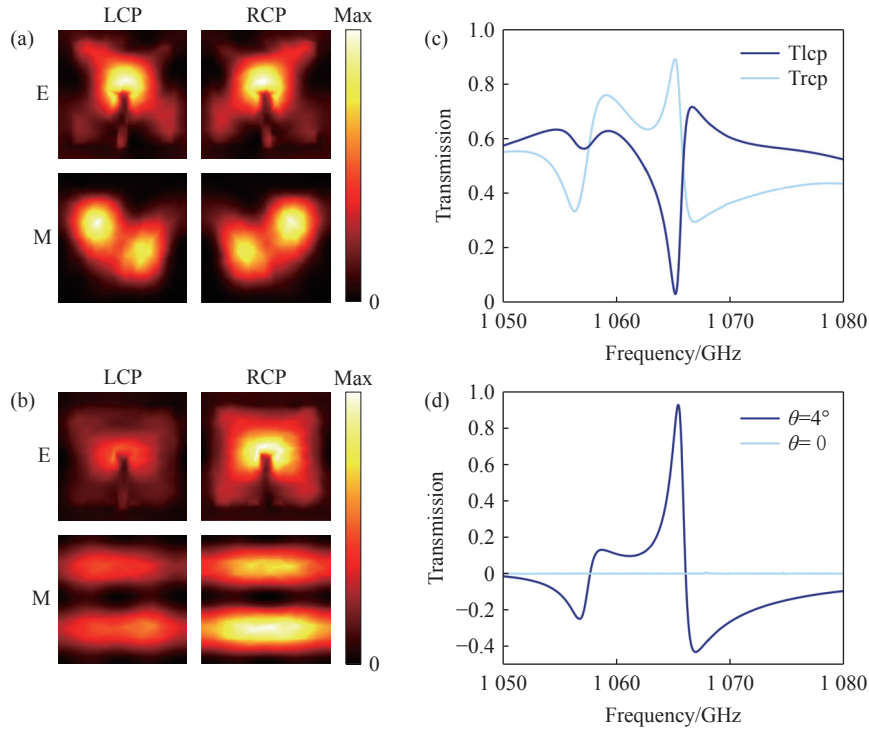


Fig. 4 The electric and magnetic field excitations at the target frequency under two incident conditions (a) incident angle $\theta = 0^\circ$. (b) incident angle $\theta = 4^\circ$. (c) Transmission coefficients of the two circularly polarized light (CPL) under oblique incidence. (d) Circular dichroism of the metasurface under two incident angles.

Simultaneously, the chirality of the BIC metasurface exhibits a strong correlation with the angle of incident light. This behavior originates from symmetry-protected BICs and is governed by two principal factors:

(1) Symmetry-Breaking-Induced Chiral Response: At normal incidence, the mirror symmetry of the structure is preserved, resulting in $CD \approx 0$.

Under oblique incidence at an angle θ , the mirror inversion symmetry is broken, effectively introducing a tilted chiral potential to the system. This creates a differential coupling strength between the LCP and RCP light to the same resonant mode, generating a CD signal that varies with θ and reaches an extremum at a specific angle. (2) BIC-to-Quasi-BIC Transition and Radiative Control: At normal incidence,

the BIC is symmetry-protected and decoupled from radiation channels, exhibiting an extremely high Q factor with negligible radiative loss. Oblique incidence breaks this symmetry, converting the BIC into a quasi-BIC with substantial radiative loss, which scales approximately with θ^2 . Consequently, the resonance depth, linewidth, and peak position become continuously tunable with the incident angle. As the chiral resonance is primarily dominated by magnetic dipole modes that are highly sensitive to the angle, the CD peak position and intensity exhibit

significant variation with θ .

Fig. 5(a) illustrates the angular dependence of maximum CD with incident angle θ , where the peak CD value occurs at $\theta = 4^\circ$. Fig. 5(b) demonstrates the spectral evolution of CD as θ varies, showing a gradual enhancement of CD from zero to the maximum values. The observed symmetrical crescent-shaped patterns demonstrate the system's transition from a non-chiral BIC to a quasi-BIC exhibiting pronounced extrinsic chirality.

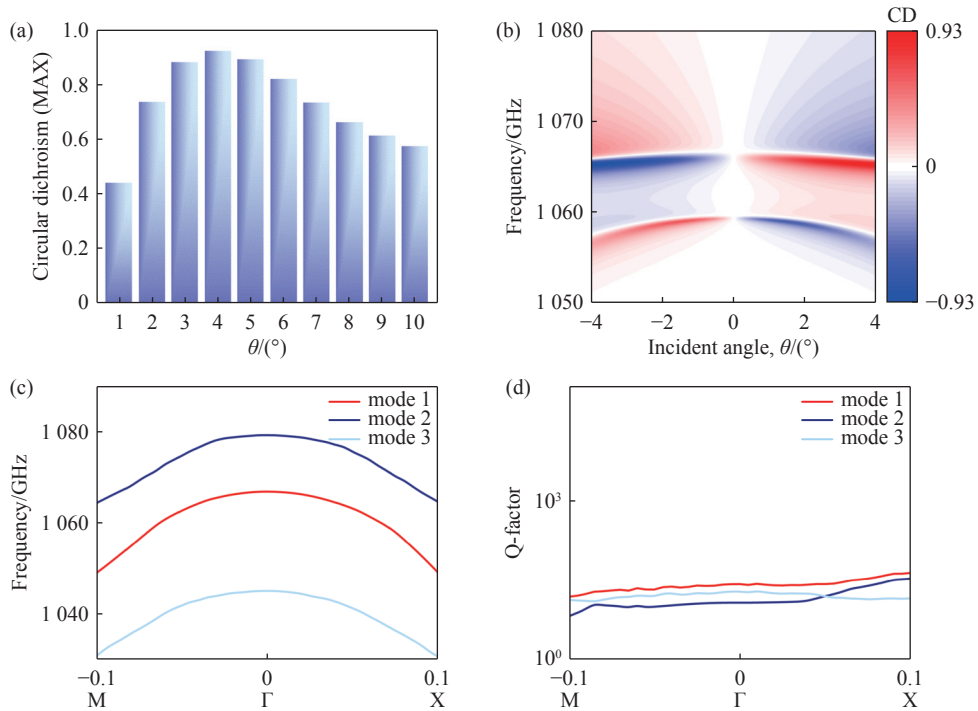


Fig. 5 (a) Maximum values of CD at various incident angles. (b) CD spectra under different incident angles. (c) Dispersion and (d) Q-factor curves of metasurface units under pumping conditions.

Subsequently, we investigate the chirality tuning mechanism through photoconductive modulation. This mechanism arises from the photoexcitation of free carriers in silicon, which alters the conductivity from 0 S/m to 12 S/m. The change in conductivity perturbs the BIC state, which is highly sensitive to such variations, leading to the destabilization and consequent degradation of the chiral response. Eigenmode analysis with Q-factor calculations was performed under 4° oblique incidence. Figs. 5(c-d) present the corresponding eigenmode dispersion and Q-factor near the target frequency,

where the disappearance of pronounced Q-factor peaks confirms the BIC annihilation.

Upon optical pumping, the carrier density in photosensitive silicon surges, leading to a marked increase in its electrical conductivity. This subsequently perturbs and ultimately extinguishes the delicate BIC mode. We aim to leverage this mechanism to achieve active switching and tuning of chirality.

Fig. 6 systematically characterizes the chirality modulation through conductivity variation. The circular dichroism (CD) value is calculated using

Eq. (1). The transmission coefficients for RCP and LCP under different conductivity states are compared in Figs. (a)-(b), revealing progressive attenuation of chiral response as conductivity increases. The corresponding evolution in Fig. 6(c) reveals a reduction in the steepness of the CD peak with increasing conductivity. Fig. 6(d) reveals a decline in

the CD peak at the target frequency with rising conductivity, demonstrating complete chirality annihilation at 12 S/m conductivity. These observations collectively confirm the feasibility of chirality switching from maximal to minimal states.

$$CD = T_L - T_R = (|t_{ll}|^2 + |t_{rl}|^2) - (|t_{rr}|^2 + |t_{lr}|^2) \quad . \quad (1)$$

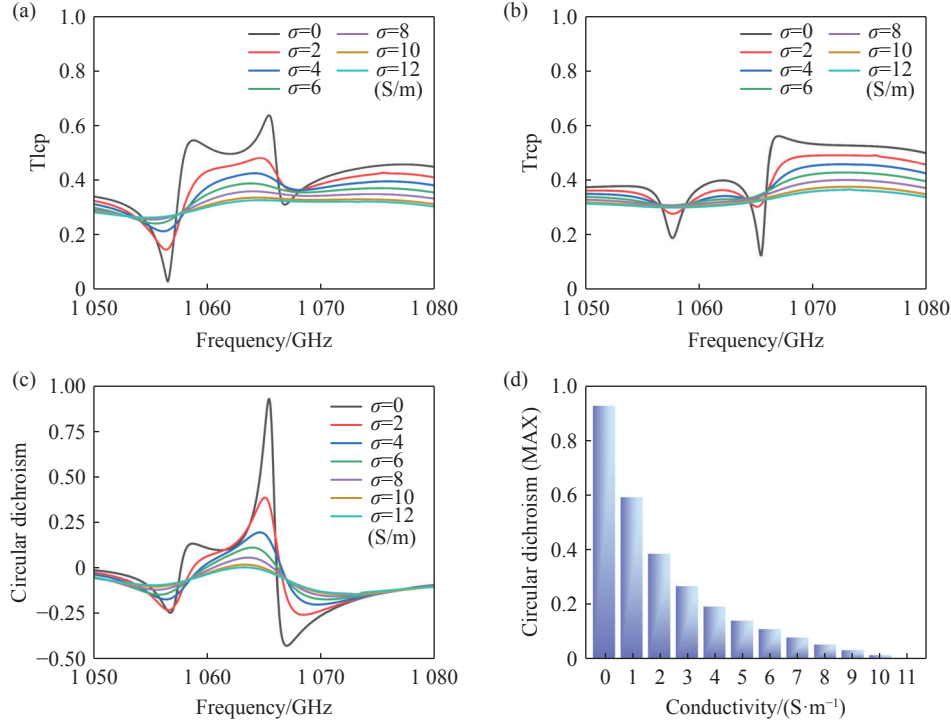


Fig. 6 Transmission coefficients for (a) LCP and (b) RCP at various conductivities. (c) CD Spectra of the metasurface at different conductivities. (d) Peak CD values of the metasurface at various conductivities.

4 Conclusion

In summary, this work presents an all-dielectric chirality-tunable metasurface based on the BIC mechanism, consisting of a quartz substrate and an array of photosensitive silicon pillars. The proposed metasurface exhibits significant chirality ($CD = 0.93$) under 4° oblique incidence. Crucially, the chirality can be dynamically switched by modulating the conductivity of the photosensitive silicon us-

ing an external pump laser. As demonstrated, when the silicon's conductivity is tuned from 0 S/m to 12 S/m, the external chirality response diminishes dramatically from its maximum value to near zero. In our future work, we plan to fabricate the structures via deep silicon etching and characterize the stability of their operational performance. This will allow us to explore the potential for achieving more complex dynamic chiral functionalities and applications, including their possible use in precision instruments and terahertz communication systems.

References:

- [1] LI J, LU X G, LI H, *et al.*. Racemic dielectric metasurfaces for arbitrary terahertz polarization rotation and wavefront manipulation[J]. *Opto-Electronic Advances*, 2024, 7(10): 240075.

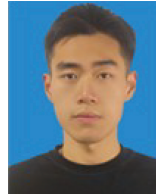
- [2] HAN Z X, WANG F, SUN J H, *et al.*. Recent advances in ultrathin chiral metasurfaces by twisted stacking[J]. *Advanced Materials*, 2023, 35(3): 2206141.
- [3] CHEN H T, TAYLOR A J, YU N F. A review of metasurfaces: physics and applications[J]. *Reports on Progress in Physics*, 2016, 79(7): 076401.
- [4] LI J, CHEN L L, XU H, *et al.*. Spin-dependent terahertz wavefront shaping based on hybrid phase in all-silicon chiral metasurfaces[J]. *Photonics Research*, 2025, 13(5): 1271-1281.
- [5] SERSIC I, VAN DE HAAR M A, ARANGO F B, *et al.*. Ubiquity of optical activity in planar metamaterial scatterers[J]. *Physical Review Letters*, 2012, 108(22): 223903.
- [6] SCHÄFERLING M, DREGELY D, HENTSCHEL M, *et al.*. Tailoring enhanced optical chirality: design principles for chiral plasmonic nanostructures[J]. *Physical Review X*, 2012, 2(3): 031010.
- [7] PLUM E, LIU X X, FEDOTOV V A, *et al.*. Metamaterials: optical activity without chirality[J]. *Physical Review Letters*, 2009, 102(11): 113902.
- [8] LI J, ZHENG CH L, WANG G C, *et al.*. Circular dichroism-like response of terahertz wave caused by phase manipulation via all-silicon metasurface[J]. *Photonics Research*, 2021, 9(4): 567-573.
- [9] HU ZH P, SUN Y W, DONG H G, *et al.*. Recent advances in dielectric chiral metasurfaces[J]. *Advanced Physics Research*, 2025, 4(6): 2400187.
- [10] SINGH R, PLUM E, ZHANG W L, *et al.*. Highly tunable optical activity in planar achiral terahertz metamaterials[J]. *Optics Express*, 2010, 18(13): 13425-13430.
- [11] MA ZH J, LI Y, LI Y, *et al.*. All-dielectric planar chiral metasurface with gradient geometric phase[J]. *Optics Express*, 2018, 26(5): 6067-6078.
- [12] HSU C W, ZHEN B, STONE A D, *et al.*. Bound states in the continuum[J]. *Nature Reviews Materials*, 2016, 1(9): 16048.
- [13] KOSHELEV K, FAVRAUD G, BOGDANOV A, *et al.*. Nonradiating photonics with resonant dielectric nanostructures[J]. *Nanophotonics*, 2019, 8(5): 725-745.
- [14] SADRIEVA Z, FRIZYUK K, PETROV M, *et al.*. Multipolar origin of bound states in the continuum[J]. *Physical Review B*, 2019, 100(11): 115303.
- [15] LI L SH, ZHANG J, WANG CH, *et al.*. Optical bound states in the continuum in a single slab with zero refractive index[J]. *Physical Review A*, 2017, 96(1): 013801.
- [16] KUPRIANOV A S, XU Y, SAYANSKIY A, *et al.*. Metasurface engineering through bound states in the continuum[J]. *Physical Review Applied*, 2019, 12(1): 014024.
- [17] KODIGALA A, LEPETIT T, GU Q, *et al.*. Lasing action from photonic bound states in continuum[J]. *Nature*, 2017, 541(7636): 196-199.
- [18] LIANG Y, KOSHELEV K, ZHANG F CH, *et al.*. Bound states in the continuum in anisotropic plasmonic metasurfaces[J]. *Nano Letters*, 2020, 20(9): 6351-6356.
- [19] LIU X Y, LI F Y, LI Y X, *et al.*. Terahertz metasurfaces based on bound states in the continuum (BIC) for high-sensitivity refractive index sensing[J]. *Optik*, 2022, 261: 169248.
- [20] KOSHELEV K, LEPESHOV S, LIU M K, *et al.*. Asymmetric metasurfaces with high- Q resonances governed by bound states in the continuum[J]. *Physical Review Letters*, 2018, 121(19): 193903.
- [21] LIU M K, POWELL D A, GUO R, *et al.*. Polarization-induced chirality in metamaterials via optomechanical interaction[J]. *Advanced Optical Materials*, 2017, 5(16): 1600760.
- [22] EVLYUKHIN A B, BOZHEVOLNYI S I, PORS A, *et al.*. Detuned electrical dipoles for plasmonic sensing[J]. *Nano Letters*, 2010, 10(11): 4571-4577.
- [23] LIM W X, SINGH R. Universal behaviour of high- Q Fano resonances in metamaterials: terahertz to near-infrared regime[J]. *Nano Convergence*, 2018, 5(1): 5.
- [24] FEDOTOV V A, ROSE M, PROSVIRNIN S L, *et al.*. Sharp trapped-mode resonances in planar metamaterials with a broken structural symmetry[J]. *Physical Review Letters*, 2007, 99(14): 147401.
- [25] KHARDIKOV V V, IARKO E O, PROSVIRNIN S L. Trapping of light by metal arrays[J]. *Journal of Optics*, 2010, 12(4): 045102.

- [26] SINGH R, AL-NAIB I A I, YANG Y P, *et al.* . Observing metamaterial induced transparency in individual Fano resonators with broken symmetry[J]. *Applied Physics Letters*, 2011, 99(20): 201107.

Author Biographies:



YANG Yue (1993—), female, born in Handan, Hebei Province, Ph.D., She received her Ph.D. from Tianjin University in 2021. Currently serves as Lecturer at Tianjin Chengjian University, She is mainly engaged in research of terahertz wave manipulation, and the design and realization of metasurfaces. E-mail: yangyue194@tju.edu.cn



YAO Bu-yi (2000—), male, born in Anqing, Anhui Province, Master's student at Tianjin University. His research focuses on the design and realization of metasurfaces. E-mail: yaobuyi@tju.edu.cn